Temperature distribution in the high mountain regions on the Tibetan Plateau - Measurement and simulation

Du M.,[1] S. Kawashima,[1] S. Yonemura, [1] T. Yamada,[2] X. Zhang,[3] J. Liu[4], Y. Li,[5] S. Gu[5] and Y. Tang[6]

[1] Department of Agro- Meteorology, National Institute for Agro-Environmental Sciences, Japan
[2] Yamada Science & Art Corporation, New Mexico, USA
[3] Institute of Geographic Sciences and Natural Resources Research, Chinese Academy of Sciences, China
[4]Institute of Tibetan Plateau, Chinese Academy of Sciences, China
[5]Northwest Institute of Plateau Biology, Chinese Academy of Sciences, China
[6] National Institute for Environmental Studies, Japan
Email: dumy@affrc.go.jp

Keywords: *Meteorological characteristics, Mountain, Temperature inversion, Tibetan Plateau*

EXTENDED ABSTRACT

The Tibetan Plateau (TP), the highest and largest plateau on Earth is characterized by very complex terrain and 1/3 of the plateau is over 4800m a.s.l. However, there are no meteorological observatories in the mountain area over 4800m. Ten simple automatic meteorological systems were set on a south facing mountain slope from 4300m to 5530m in the central part of the TP. The observation shows an uniform lapse rate about 0.69 °C/100m along the slope, in summertime. The lapse rate is a little bit greater than that of averaged over the TP. However, there is a very lower lapse rate about 0.09°C/100m at lower portion of slope (below 4800m) and a relatively larger lapse rate about 0.9°C/100m at higher portion of the slope in wintertime. Due to strong radiation cooling based on lower humidity and cold air run-off from a higher mountain region into the valley or basin by a local circulation, the air temperature in the valley or basin becomes lower and lower during night in wintertime. This process occurred and a temperature inversion layer exited almost every day during wintertime. The temperature inversion was formed around sunset (before 20:00 BST, local time is about 2 hours earlier) and developed gradually until next morning. Inversion layer reached to 5100m at about 8:00 BST and disappeared rapidly after sunrise.

The averaged lapse rate for the TP (calculated by using thirty years (1950-1080) mean air temperature of 85 stations) is 0.57 °C/100m in July and 0.56 °C/100m in January. Our observation shows a greater lapse rate about 0.69°C/100m along the slope in July. This may be the effect of higher temperature between 4400m to 4800m. Our observed lapse rate in winter was completely different from the average due to the existence of temperature inversion.

The YSA's (Yamada Science and Art) A2C atmospheric modeling solution (NEW HOTMAC model) is used for illustrating this local circulation. The HOTMAC Model gives very clear result that the local circulation in the mountain has an effect on the vertical profile of air temperature in wintertime.

On the other hand, The TP has been considered to be one of the most ecologically fragile and sensitive ecosystems on the earth. Grassland occupies about 50% of the Tibetan Plateau and distribute even to 5200m a.s.l. in high mountain region. An over three times increasing in livestock production in the Tibetan Plateau has occurred since 1978. Historical meteorological data showed that the elevation of air temperature on the Tibetan Plateau is greater than for the whole China and East Asia within the same period. In our observation site, vegetation cover as well as species number and root biomass in the lower part of the slope below 4600m is much lower than that around 5000m. The decrease of species number, vegetation cover and root biomass may be related to the grazing pressure. These may have had effect on the temperature distribution in our observation results such as increasing air temperature in lower part of the slope. Therefore, the lapse rate is a little bit greater than the average in summertime. Meteorological observatories' data on the TP is not ideal for assessing meteorological characteristics in high mountain regions, especially for wintertime. Human activities (mainly grazing) may have great effect on the temperature distribution. Long-term meteorological observation and ecological investigation in high mountain region will be very important in high mountain regions in the future.

1. INTRODUCTION

The Tibetan Plateau (or Qinghai-Xizang Plateau, hereafter TP) is the highest (averaging >4000m) and largest plateau on Earth. The TP is characterized by very complex terrain and 1/3 of the plateau is over 4800m. TP is of immense importance both to climate and to ecosystems of the Asian continent and even the whole world. Research on the climate change in the TP has received increasing attention since mid-1970s (e.g. Zheng et al., 2000). There is strong evidence that the TP exerts profound thermal and dynamical influences on the local weather and climate as well as on atmospheric circulation (e.g. Manabe and Terpstra, 1974) and some studies suggest that the TP is one of the most sensitive areas to respond to global climate change (e.g. Liu and Chen, 2000). Liu and Chen (2000) showed that the main portion of the TP has experienced statistically significant warming since the mid-1950s, especially in winter, which exceed those for the Northern Hemisphere and the same latitudinal zone in the same period. Most of the works concerning climate change in the TP attempt to link the climate change to atmospheric circulations or global warming related to the atmosphere greenhouse gases (e.g. Yin et al., 2000; Liu and Chen, 2000).

However, the meteorological observatories on the TP are biased to the populated lower-elevation area (<4800m) in the eastern and southern TP. Observational data is not ideal for assessing long-term trends on the TP (Frauenfeld et al., 2005). The results obtained from the studies described above can only represent the available data sources they used. They indicate an obvious warming climate on the TP in recent decades. Frauenfeld et al. (2005), however, found that there are no significant trends on the TP in its 2-m temperature from European Centre for Medium-Range Weather Forecasts (ECMWF) Reanalysis (ERA40; Simmons and Gibson, 2000). Kalnay and Cai (2003) suggested a potential explanation for the difference between reanalysis and station trend is the extensive local and regional land use changes during recent decades. Du et al. (2004) suggested that degradation of grassland by over grazing on the TP should have an effect on the climate change on the TP. This may be one of the reasons why climate warming on the TP is greater than on other places. Therefore, it is very important to know the meteorological characteristics, especially the temperature distribution and variation in the unpopulated higher-elevation area (>4800m) on the TP. This paper shows some observational results of temperature distribution on a mountain slope from 4300m to 5530m a.s.l. in the central part on the TP and simulation result for clarifying the local circulation effect on the temperature distribution.

2. OBSERVATIONS

2.1. Observation site

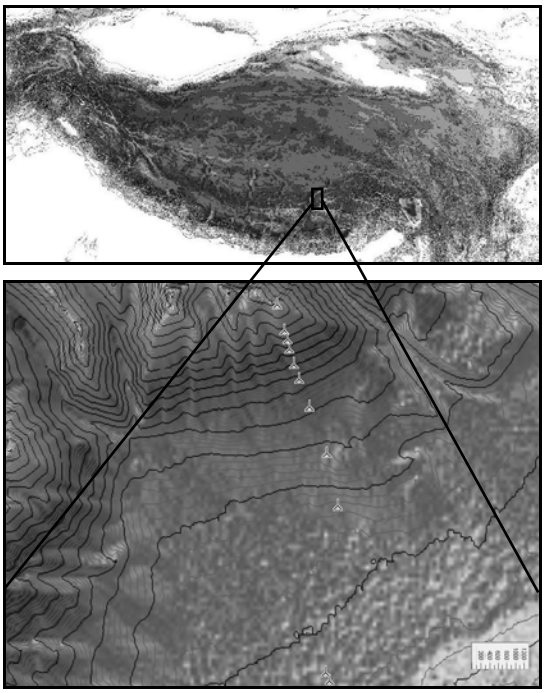

Figure 1. The main topography over the Tibetan Plateau (up) and observation stations (down). The Tibetan Plateau is shown as the shaded region where elevation is higher than 3000 m a.s.l.. Black contour lines show topography with an interval of 1000 m (up) and 100m (down). The triangles indicate the observation stations.

Figure 1 shows the main topography over the TP and the observation sites. There are no meteorological observatories in the area over 4800m a.s.l. which occupied 1/3 of TP showed as dark areas in Figure 1 (up). We set up 11 observation stations on a south slope of Mount Nyainqentanglha as shown in Figure 1 (down) at Dangxiong (30°28-32'N, 91°02-03'E). One of the 11 stations is a basic automatic station at about 4300m in the valley (hereafter AWS). All the meteorological elements including short and long wave radiations, wind speed and direction, air temperature and humidity, soil temperature and water content etc. were measured there by using measurement system of Campbell Scientific, Inc. Data were recorded with a data-logger (CR10X; CSI) at 30 min intervals. Measurement system on the other 10 stations are Hobo weather stations (Onset Computer Corporation) settled at 4300m, 4400, 4500m, 465m, 4800m, 4950m, 5100m, 5200m 5300m 5530m on a south slope. Air temperature and humidity at 2m and soil temperature and soil water content at 5cm, 20cm and 50cm are sampled at 1 min intervals and the mean value were recorded with a data-logger at

30 min intervals. The air temperature data from August 2005 to January 2007 are presented in this study.

2.2. Daily mean air temperature distribution

Figure 2 shows daily mean air temperature distribution with height during one year from Aug. 6, 2005 to Aug. 5, 2006. Temperature decreased gradually with height in summer (Jun. to Aug.). However, there was a height where daily mean air temperature was higher than that in the lower places. A temperature inversion layer exited along the lower part of the slope. The inversion height became higher and higher gradually from middle of November to late of December and disappeared rapidly in April. Inversion height was about 500m high (about 4800m) in January.

2.3. Temperature profiles

Monthly mean air temperature profile also shows a clear temperature inversion during wintertime as shows in Figure 3. Figure 3 shows an uniform lapse rate about 0.69 ^{0}C/100m along the slope in summer (July and August) and early autumn (September) and shows a very lower lapse rate about 0.09 ^{0}C/100m at lower part of slope (below 4800m) and a relatively larger lapse rate about 0.9 ^{0}C/100m at higher part of the slope in wintertime.

2.4. Formation of air temperature inversion

As mentioned above, air temperature inversion existed almost every day during winter in our observation area. Figure 4 shows an example of the formation and variation of the air temperature inversion during Jan. 8 to 9, 2007. A temperature inversion was formed around sunset (before 20:00 BST, local time is about 2 hours earlier) and developed gradually until next morning. Inversion layer reached to 5100m at about 8:00 BST and disappeared rapidly after sunrise. Figure 5 gives the diurnal variation of solar radiation, net radiation, relative humidity, wind speed and direction for the same period. It can be concluded that this was a typical nocturnal invasion by radiation cooling in a valley. After sunset (solar radiation changes to zero), net radiation changed form plus (heating effect) to minus (cooling effect) and wind speed decreased rapidly. After several hours cooling, inversion layer became thinker and thinker and wind direction changed from SSW, valley wind to NNE, wind from the mountain slope.

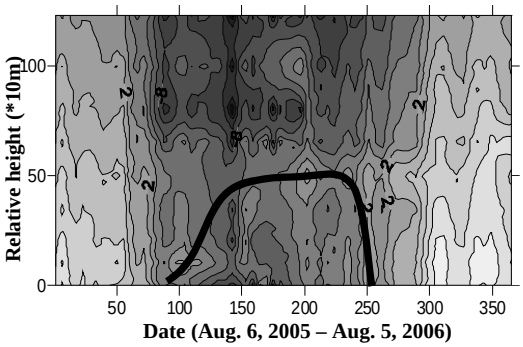

Figure 2. Daily mean air temperature distribution with height along a south slope at Dangxiong, TP during one year from Aug. 6, 2005 to Aug. 5, 2006. The bold line indicates the warm centre on the slope in wintertime.

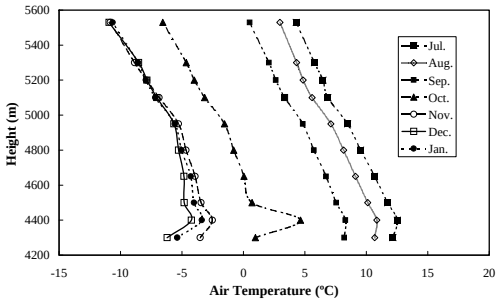

Figure 3. Variation of monthly mean temperature profiles along the south slope from July 2006 to January 2007.

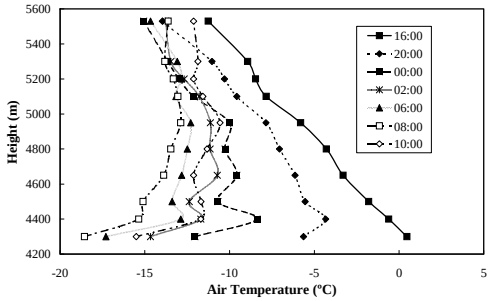

Figure 4. Variation of air temperature profiles along the south slope from 16:00 BST Jan. 8, 2007 to 10:00 BST Jan. 9, 2007.

2.5. Cause of temperature inversion

As mentioned above, our observed temperature inversion is a nocturnal inversion in valley or basin mainly deduce by nocturnal radiation cooling. Usually, this kind of temperature inversion occurs on clear calm night. It is well known that calm day is not prevailing on the TP, especially in wintertime. As shown in figure 5, the wind speed at our valley station was more than 1m/s in the night. It seems that certain wind can accelerate heat exchange within a valley or basin and let the inversion layer developed to a higher place.

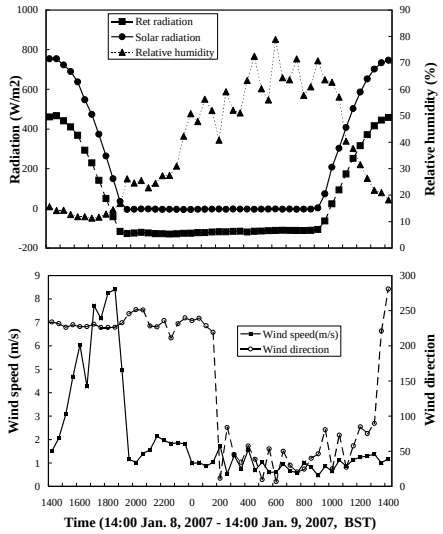

Figure 5. Diurnal variation of solar radiation, net radiation, relative humidity, wind speed and direction on Jan. 8-9, 2007.

In order to clarify the cause of temperature inversion on TP to explain why the inversion was existed only in wintertime, daytime (from 10:00 to 20:00 BST) and night time (21:00 to 8:00 BST next day) value of radiation, humidity and wind were calculated. Figure 6 shows annual variation of net radiation, relative humidity and wind speed for daytime and night time. We can see that although wind speed of daytime was much greater in wintertime, wind speed at night time was similar as summertime. Ret radiation at night time was very lower in wintertime and relative humidity (both daytime and night time) was lower than summertime. Compared with Figure 2, strong radiation cooling under relative dry condition is the main cause for the temperature inversion.

2.6. Comparison of the lapse rate along the slope to that of averaged over the TP

Thirty years (1950-1080) mean air temperature of 85 stations was used for calculating the averaged lapse rate by removing latitude and longitude effect. Figure 7 shows the relationship between mean air temperature and height for these 85 stations. Our observation results were also showed in Figure 7. The averaged lapse rate for the TP is 0.57 ^{0}C/100m in July and 0.56 ^{0}C/100m in January. Our observation shows a greater lapse rate about 0.69^{0}C/100m along the slope in July. This may be the effect of higher temperature between 4400m to 4800m. Our observed lapse rate in winter was completely different from the average due to the existence of temperature inversion.

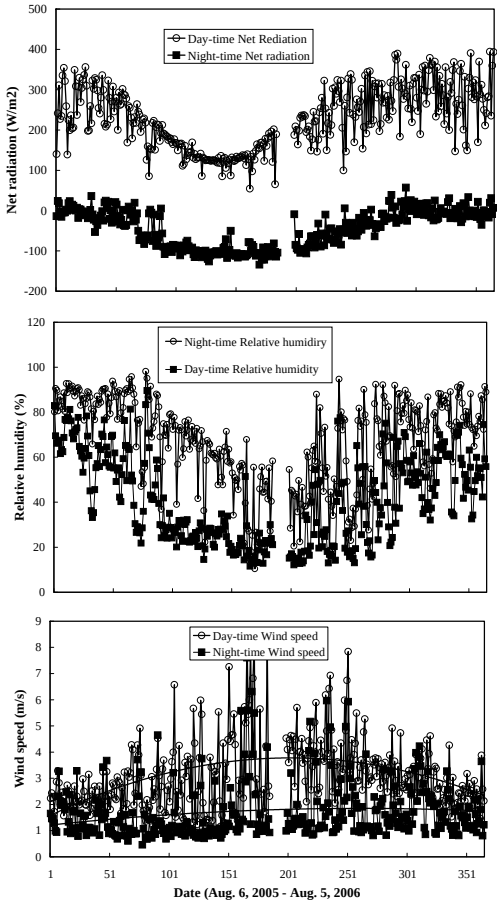

Figure 6. Annual variation of net radiation, relative humidity and wind speed for daytime and night time (from Aug. 6, 2005 to Aug. 5, 2006)

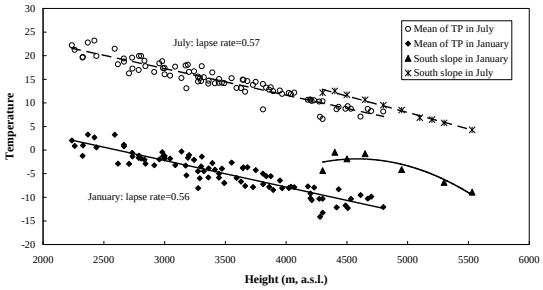

Figure 7. Relationship between air temperature and height on the TP in July and January.

All the meteorological observatories on the Tibetan Plateau are biased to the populated lower-elevation area in valleys or basins lower than 4800m. Therefore, meteorological observatories' data is not ideal for assessing meteorological characteristics in high mountain region, especially for wintertime.

2.7. Importance of temperature distribution on high mountain regions

The TP has been considered to be one of the most ecologically fragile and sensitive ecosystems on the earth. Grassland occupies about 50% of the Tibetan Plateau and distribute even to 5200m a.s.l. in high mountain region. An over three times increasing in livestock production in the Tibetan Plateau has occurred since 1978 (Du et al., 2004). However, degradation (such as vegetation cover decreasing) of grassland due to over grazing on the TP has been a problem (Zhu and Li, 2000). Decreasing in vegetation cover reduces evapotranspiration thereby allowing an increase in local temperature levels (e.g. Du, 1996, Balling et al., 1998). In our observation site, vegetation cover as well as species number and root biomass in the lower part of the slope below 4600m is much lower than that around 5000m. The decrease of species number, vegetation cover and root biomass may be related to the grazing pressure. These may have had effect on the temperature distribution in our observation results such as increasing air temperature in lower part of the slope. Therefore, the lapse rate is a little bit greater than the average in summertime. Long-term meteorological observation and ecological investigation will be very important in the future.

3. SIMULATIONS

3.1. Model equations

Since our wind observation is only obtained by AWS at the valley, we used the New HOTMAC model (Yamada Science and Art) to simulate the local circulation. The basic HOTMAC equations for mean wind, temperature, mixing ratio of water vapour, and turbulence are similar to those used by Yamada and Bunker (1988).

In order to accurately treat surface boundary conditions, a terrain-following vertical coordinate system is used:

$$z^* = \overline{H}\frac{z - z_g}{H - z_g}, \tag{1}$$

where z^* and z are the transformed and Cartesian vertical coordinates, respectively; z_g is ground elevation; $\overline{H}$ is the material surface top of the model in the z^* coordinate and H is the corresponding height in the z coordinate.

The governing equations following the coordinate transformation are

$$\frac{DU}{Dt} = f(V - V_g) + g\frac{\overline{H} - z^*}{\overline{H}}\left(1 - \frac{\langle\Theta_v\rangle}{\Theta_v}\right)\frac{\partial z_g}{\partial x} + \frac{\partial}{\partial x}\left(K_x\frac{\partial U}{\partial x}\right) + \frac{\partial}{\partial y}\left(K_{xy}\frac{\partial U}{\partial y}\right) + \frac{\overline{H}}{H - z_g}\frac{\partial}{\partial z^*}\left(-\overline{uw}\right), \tag{2}$$

$$\frac{DV}{Dt} = f(U - U_g) + g\frac{\overline{H} - z^*}{\overline{H}}\left(1 - \frac{\langle\Theta_v\rangle}{\Theta_v}\right)\frac{\partial z_g}{\partial y} + \frac{\partial}{\partial x}\left(K_{xy}\frac{\partial V}{\partial x}\right) + \frac{\partial}{\partial y}\left(K_y\frac{\partial V}{\partial y}\right) + \frac{\overline{H}}{H - z_g}\frac{\partial}{\partial z^*}\left(-\overline{vw}\right), \tag{3}$$

$$\frac{\partial U}{\partial x} + \frac{\partial V}{\partial y} + \frac{\partial W^*}{\partial z^*} - \frac{1}{H - z_g}\left(U\frac{\partial z_g}{\partial x} + V\frac{\partial z_g}{\partial y}\right) = 0, \tag{4}$$

$$\text{where } W^* \equiv \frac{\overline{H}}{H - z_g}W + \frac{z^* - \overline{H}}{H - z_g}\left(U\frac{\partial z_g}{\partial x} + V\frac{\partial z_g}{\partial y}\right), \tag{5}$$

$$\text{and } \frac{\mathrm{D}(\,)}{\mathrm{D}t} \equiv \frac{\partial(\,)}{\partial t} + U\frac{\partial(\,)}{\partial x} + V\frac{\partial(\,)}{\partial y} + W^*\frac{\partial(\,)}{\partial z^*}. \tag{6}$$

In the above expressions, U, V, and W are velocity components in x, y, and z directions, respectively, $\langle\ \rangle$ indicates an average over a horizontal surface. The second terms on the right-hand side of eqs. (2) and (3) indicate the effects of ground slope, which are resulted from the coordinate transformation.

For simplicity, H is specified as

$$H = \overline{H} + z_{g\max} \tag{7}$$

where z_{gmax} is the max height of ground elevation in the study area.

The geostrophic winds U_g and V_g are computed from

$$fU_g \equiv fU_g\left(\overline{H}\right)\frac{\langle\Theta_v\rangle}{\left\langle\Theta_v\left(\overline{H}\right)\right\rangle} + g\frac{H - z_g}{\overline{H}}\int_{z_s}^{\overline{H}}\frac{1}{\langle\Theta_v\rangle}\frac{\partial\Delta\Theta_v}{\partial y}dz' - \frac{g}{H}\frac{\partial z_g}{\partial y}\int_{z_s}^{\overline{H}}\frac{\Delta\Theta_v}{\langle\Theta_v\rangle}dz', \tag{8}$$

and

$$fV_g \equiv fV_g\left(\overline{H}\right)\frac{\langle\Theta_v\rangle}{\left\langle\Theta_v\left(\overline{H}\right)\right\rangle} - g\frac{H - z_g}{\overline{H}}\int_{z_s}^{\overline{H}}\frac{1}{\langle\Theta_v\rangle}\frac{\partial\Delta\Theta_v}{\partial x}dz' + \frac{g}{H}\frac{\partial z_g}{\partial x}\int_{z_s}^{\overline{H}}\frac{\Delta\Theta_v}{\langle\Theta_v\rangle}dz', \tag{9}$$

where $\Delta\Theta_v \equiv \Theta_v - \langle\Theta_v\rangle$, and the abbreviated symbols $U_g\left(\overline{H}\right) \equiv U_g(x, y, \overline{H}, t)$, $V_g\left(\overline{H}\right) \equiv V_g(x, y, \overline{H}, t)$, etc., are used.

A turbulence kinetic energy equation is given by

$$\frac{D}{Dt}\left(\frac{q^2}{2}\right) = \frac{\partial}{\partial x}\left[K_x\frac{\partial}{\partial x}\left(\frac{q^2}{2}\right)\right] + \frac{\partial}{\partial y}\left[K_y\frac{\partial}{\partial y}\left(\frac{q^2}{2}\right)\right] + \left(\frac{\overline{H}}{H - z_g}\right)^2\frac{\partial}{\partial z^*}\left[qlS_q\frac{\partial}{\partial z^*}\left(\frac{q^2}{2}\right)\right] - \frac{\overline{H}}{H - z_g}\left(\overline{uw}\frac{\partial U}{\partial z^*} + \overline{vw}\frac{\partial V}{\partial z^*}\right) + \beta g\,\overline{w\theta}_v - \frac{q^3}{B_1 l} \tag{10}$$

and a turbulence length scale l is obtained from

$$\frac{D}{Dt}\left(q^2 l\right) = \frac{\partial}{\partial x}\left[K_x\frac{\partial}{\partial x}\left(q^2 l\right)\right] + \frac{\partial}{\partial y}\left[K_y\frac{\partial}{\partial y}\left(q^2 l\right)\right] + \left(\frac{\overline{H}}{H - z_g}\right)^2\frac{\partial}{\partial z^*}\left[qlS_l\frac{\partial}{\partial z^*}\left(q^2 l\right)\right] + lF_1\left[\frac{\overline{H}}{H - z_g}\left(-\overline{uw}\frac{\partial U}{\partial z^*} - \overline{vw}\frac{\partial V}{\partial z^*}\right) + \beta g\,\overline{w\theta}_v\right]$$

$$-\frac{q^3}{B_1}\left[1+F_2\left(\frac{1}{kz}\right)^2\right] \quad (11)$$

where $q^2 = \overline{u^2} + \overline{v^2} + \overline{w^2}$ is twice the turbulence kinetic energy, $\overline{w\theta}_v$ turbulence heat flux, θ_v the fluctuation part of virtual potential temperature, and (F_1, F_2, S_q, S_l, and B_1) = (1.8, 1.33, 0.2, 0.2, and 16.6) empirical constants determined from laboratory experiments (Mellor and Yamada, 1982).

The internal heat energy equation is written as

$$\frac{D\Theta}{Dt} = \frac{\partial}{\partial x}\left[K_x\frac{\partial\Theta}{\partial x}\right] + \frac{\partial}{\partial y}\left[K_y\frac{\partial\Theta}{\partial y}\right] + \frac{\overline{H}}{H-z_g}\left[\frac{\partial}{\partial z^*}\left(-\overline{w\theta}\right)\right]. \quad (12)$$

A conservation equation for mixing ratio of water vapour is given by

$$\frac{DQ_v}{Dt} = \frac{\partial}{\partial x}\left[K_x\frac{\partial Q_v}{\partial x}\right] + \frac{\partial}{\partial y}\left[K_y\frac{\partial Q_v}{\partial y}\right] + \frac{\overline{H}}{H-z_g}\frac{\partial}{\partial z^*}\left(-\overline{wq}_v\right). \quad (13)$$

The turbulent fluxes in eqs. (2), (3), (10), (11), (12), and (13) are obtained from simplified second-moment turbulence-closure equations (Yamada, 1983)

3.2. Simulations

We deployed nested grids 3 of domains to include both large topography (a part of Mount Nyainqentanglha) and small topography (only the valley and the slope where observation obtained) as shown in Figure 8. Simulations initiated at 14:00 Jan. 8 and stoped at 14:00 Jan. 10. Initial wind directions were westerly (250°) and wind speeds in the upper levels were 2 m/s. Potential temperature gradients in the vertical direction were 0.001 K/m for the first 1000 m above the ground and 0.003 K/m in the levels greater than 1000 m above the ground. The top of computational domain was 10000m above the highest ground elevation, which was 5530 m for the present study.

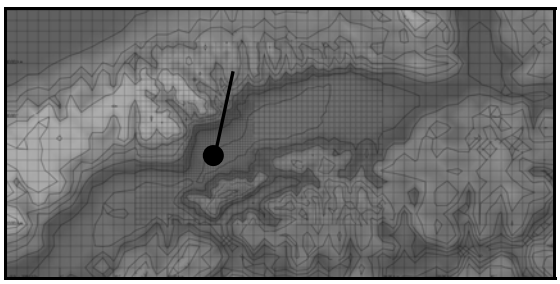

Figure 8. Grid lines and topography of computation domains. The bold line indicates observation transection and ● indicates the AWS with wind observation.

3.3. Results

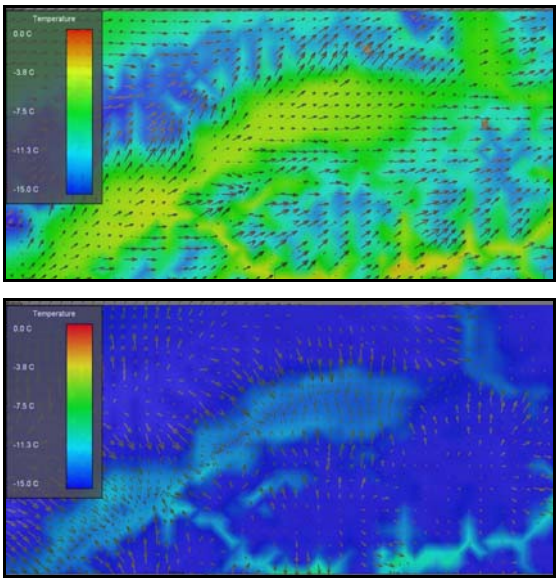

Figure 9. The modelled wind and temperature distributions in Domain 1 at 2 m above the ground (up: 16:00; down: 07:00). Arrows indicate wind directions and wind speeds are proportional to the lengths of arrows.

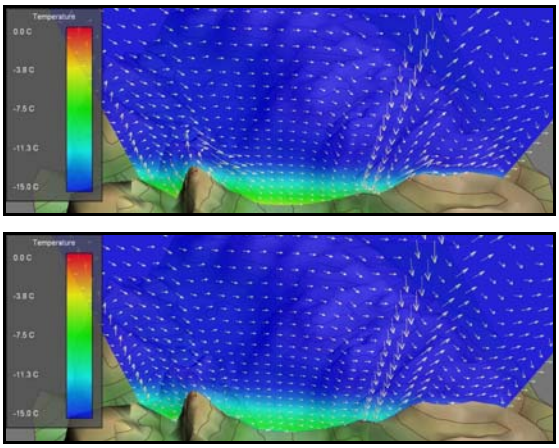

Figure 10. The modelled wind and temperature distributions in the vertical cross section along the observation slope. (up: 16:00; down: 07:00). Arrows indicate wind directions and wind speeds are proportional to the lengths of arrows.

Figure 9 shows the modelled horizontal wind distributions in domain 1 at 2 m above the ground at 16:00 and 07:00 local time. During the daytime westerly wind was proving in the whole domain area and air temperature is higher in the lower valley. As the ground began cooling, westerly breezes changed to hill breezes and upslope flows changed to down slope flows over the hills. In the valley, westerly wind changed to easterly wind due to down slope flows from both mountain sides (north wind and south wind) just like the observation as shown in Figure 5 and air temperature was lower

than that on the lower part of the mountain slope. The local circulation between mountain and valley was very thin, especially during the nigh time as shown in Figure 10. However, this circulation accelerated the cooling process in the valley (bring cold air from higher place to lower places).

4. CONCLUSIONS

In order to clarify the vertical pattern of air temperature in high mountain regions where no meteorological observatories, we set ten simple observation stations along a south slope from 4300m to 5530m in central part of the TP since August 2005. New HOTMAC Model (Yamada Science and Art) was used to simulate the local atmospheric circulation based on the observation in this mountain region. The observation results show that the lapse rate in summer time is similar to that of averaged over the TP. The lapse rate in winter, however, is much lower than the average for the lower portion, but much greater than that for the upper portion of the slope, which indicates a temperature inversion layer on the slope due to strong radiation cooling and local circulation system. The New HOTMAC atmospheric modelling solution can be used to simulate the local circulation and temperature profile in high mountain region. Human activities (mainly grazing) may have great effect on the temperature distribution. Long-term meteorological observation and ecological investigation will be very important in high mountain regions in the future.

5. REFERENCES

Balling Jr., R.C., Klopatek, J.M., Hildebrandt, M.L., Moritz, C.K., Watts, C.J., 1998. Impacts of land degradation on historical temperature records from the Sonoran Desert. Clim. Change, 40, 669– 681.

Du, M., 1996. Is it a global change impact that the climate is becoming better in the western part of the arid region of China? Theor. Appl. Climatol. 55, 139–150.

Du, M., Kawashima, S., Yonemura, S., Zhang, X., Chen, S., 2004. Mutual influence between human activities and climate change in the Tibetan Plateau during recent years. Glob. Planet. Change 41, 241–249.

Frauenfeld, O.W., Zhang, T., Serreze, M.C., 2005. Climate change and variability using European Centre for Medium-Range Weather Forecasts reanalysis (ERA40) temperatures on the Tibetan Plateau. J. Geophys. Res. 110, D02101. doi:10.1029/2004JD005230.

Kalnay, E., Cai, M., 2003. Impact of urbanization and land-use change on climate. Nature 423 (6939), 528–531.

Liu, X. and Chen, B., 2000. Climatic warming in the Tibetan Plateau during recent decades. Int. J. Climatol. 20 (14), 1729– 1742.

Manabe, S. and Terpstra, T.B., 1974. The effects of mountains on the general circulation of the atmosphere as identified by numerical experiments. J. Atmospheric Sciences 31 (1), 3 – 42.

Mellor, G. L., and T. Yamada, (1982), Development of a Turbulence Closure Model for Geophysical Fluid Problems; Rev. Geophys. Space Phys., 20, 851-875.

Simmons, A.J., Gibson, J.K., (2000). The ERA40 project plan. ERA40 Project Report Series No. 1. ECMWF, Reading, UK, p. 63.

Yamada, T., (1983), Simulations of Nocturnal Drainage Flows by a q^2l Turbulence Closure Model, J. of Atmos. Sci., 40, 91-106.

Yamada, T., and S. Bunker, (1988), Development of a Nested Grid, Second Moment Turbulence Closure Model and Application to the 1982 ASCOT Brush Creek Data Simulation, Journal of Applied Meteorology, 27, 562-578.

Yin, Z., Lin, Z., Zhao, X., 2000. Temperature anomalies in central and eastern Tibetan Plateau in relation to general circulation patterns during 1951–1993. Int. J. Climatol. 20 (12), 1431– 1449.

Zheng, D., Q. Zhang and S. Wu, (Eds.), (2000), Mountain Genecology and Sustainable Development of the Tibetan Plateau. Kluwer Academic Publisihing, Dordrecht.

Zhu, L., and Li, B., (2000), Natural hazards and environmental issues. In: Zheng, D., Zhang, Q., Wu, S. (Eds.), Mountain Genecology and Sustainable Development of the Tibetan Plateau. Kluwer Academic Publishing, Dordrecht, pp. 203–222.